<Original Paper>

Journal of the Korean Society for Nondestructive Testing, Vol. 34, No. 6: 457-466, 2014
ISSN 1225-7842 / eISSN 2287-402X http://dx.doi.org/10.7779/JKSNT.2014.34.6.457

Simulation of Excitation and Propagation of Pico-Second Ultrasound

Seungyong Yang* and Nohyu Kim*†

Abstract This paper presents an analytic and numerical simulation of the generation and propagation of pico-second ultrasound with nano-scale wavelength, enabling the production of bulk waves in thin films. An analytic model of laser-matter interaction and elasto-dynamic wave propagation is introduced to calculate the elastic strain pulse in microstructures. The model includes the laser-pulse absorption on the material surface, heat transfer from a photon to the elastic energy of a phonon, and acoustic wave propagation to formulate the governing equations of ultra-short ultrasound. The excitation and propagation of acoustic pulses produced by ultra-short laser pulses are numerically simulated for an aluminum substrate using the finite-difference method and compared with the analytical solution. Furthermore, Fourier analysis was performed to investigate the frequency spectrum of the simulated elastic wave pulse. It is concluded that a pico-second bulk wave with a very high frequency of up to hundreds of gigahertz is successfully generated in metals using a 100-fs laser pulse and that it can be propagated in the direction of thickness for thickness less than 100 nm.

Keywords: Pico-Second Ultrasound, Numerical Simulation, Thin Films, Uultrafast Laser Pulse, Heat Transfer

1. Introduction

Thin films and microstructures are widely used in the semiconductor industry, automotive industry, biotechnology and numerous electrical devices such as CMOS. The growing importance of electromechanical microstructures (MEMS) requires a rapid characterization during and after fabrication. Many different methods such as scanning electron microscopy (SEM) and tunneling electron microscopy (TEM) techniques provide data of roughness and surface quality and of electrical and optical properties [1]. However, the mechanical quantities are measured mostly by destructive techniques such as nano-indentation, even though it is one of key parameters for manufacturing processes and conditions in the micro-devices and performance of thin films. Since the thickness of films and coatings significantly influence the resulting mechanical properties, non-destructive measurement techniques are necessary, which can provide mechanical properties of coatings or microstructures after fabrication. Recently few nondestructive testing methods including GHz scanning electronic acoustic microscopy (SAM) and ultrasonic atomic force microscopy (UAFM) techniques were introduced and applied to MEMS [1]. In these technologies, surface waves or Lamb waves are generated on thin films via acoustic lens and micro-structured cantilever for measurement of mechanical properties of thin films. Main reason to use guided waves in SAM and UAFM is that those technologies have a limited capability in acoustic frequency, which is, at best 1 GHz, so that ultrasonic wavelength is about 1 μm. They also need a relatively complex inversion process like dispersion analysis to estimate mechanical parameters or acoustic velocity from experimental data. This limitation is a critical barrier for nondestructive evaluation of nano-scale MEMS. In order to achieve an acceptable resolution the wavelength of the acoustic pulses propagating through the structure has to be short compared

[Received: November 20, 2014, Revised: December 18, 2014, Accepted: December 24, 2014] **Dept. of Mechanical Engineering, Korea University of Technology and Education, 307 Gajun-Ri, Byungchun-Myun, Chunan 330-860, Korea
†Corresponding Author: nykim@koreatech.ac.kr

to the geometrical dimensions of the specimen. This condition becomes especially challenging when inspecting microstructures and coatings with sub-micron dimensions. The acoustic wavelength to analyze microstructures and thin films needs to be in the nanometer range. This small wavelength corresponds to acoustic pulses having frequency content beyond 100 GHz. Unlike conventional laser ultrasound, ultra-short laser pulses in femto-second scale has been proved to excite the ultra-short ultrasound of hundreds of GHz without any damage to materials [3-5]. In the papers by C. Thomsen and J. K. Chen [6-9], a theory and experiment of the excitation and detection of acoustic pulses with short laser pulses is presented well enough as long as the temperature diffusion plays a minor role or the laser pulses are not too short. Several papers about the excitation of acoustic pulses in semiconductors and microstructures is also reported [10,11]. But a very rare research on ultrafast laser-based ultrasound are found in Korea only except a joint research done by KAERI with Idaho national research center of United States in 2009.

The simulation of pico-second ultrasound consists of the thermoelastic excitation and the propagation of the acoustic pulse by combining the theoretical formulation of each part with the appropriate numerical method. Accurate numerical model for the excitation and propagation of acoustic pulses has been sought using a simple thermo-mechanical model which neglects the short duration of heat transfer by incident laser pulse [11,12]. But general numerical models especially with a calculation of the wave propagation in 1-, 2- or 3D configurations have not been realized yet.

In this paper, the excitation and propagation of acoustic pulses produced by ultra-short laser pulses are presented using an analytical model which is based on the work of Thomsen [5]. Using finite difference (FD) methods, the wave equation with thermal disturbance induced by laser is discretized and analyzed to calculate the waveforms of acoustic pulse in aluminum substrate. Numerical solutions by Matlab are discussed by comparing with analytical solutions.

2. Thermo-Dynamic Equations for Laser Induced Acoustic Pulse

If the surface of an absorbing metal in thin film or metallic microstructure is irradiated with ultra-short laser pulses having durations of less than 100fs as shown in Fig. 1, the laser pulses are absorbed within a characteristic, material dependent distance, the absorption length ζ. The absorption length ζ or penetration depth expressed by [7]

$$\zeta = \frac{\ell}{2\pi\kappa} \tag{1}$$

is calculated with the wavelength of the laser ℓ and the imaginary part of the refraction index κ of the material. The absorption depth ζ of the ultra-short laser is very small down to few nm depending on the material. For example, aluminum has a penetration depth of about 7.5 nm. The energy $E(z)$ deposited per unit volume at a distance z is given by, when a short pulse is incident on uniformly irradiated area A_s of the free surface,

$$E(z) = \frac{(1-R)}{A_s\zeta} \, Q \, e^{-\frac{z}{\zeta}} \tag{2}$$

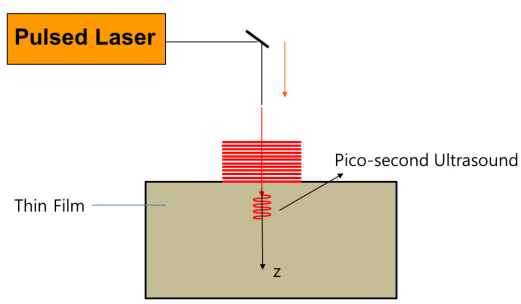

Fig. 1 Schematic diagram of acoustic generation by ultrafast pulsed laser

in which R denotes the optical reflectivity of the surface, Q the energy of the incident laser beam and ζ the penetration depth according to Eq. (1).

The area A_s of the specimen irradiated by the laser pulse is large compared to the film thickness d and the absorption length ζ. Therefore the excitation of the acoustic waves is considered in the z direction only. In general, metallic surface has absorption-lengths (penetration depth) ζ in the order of 10 to 20 nm which is three orders of magnitude smaller than the experimentally achievable spot size A_s (~5-50 μm in diameter). In principle, the temperature increase $\triangle T$ in a solid is calculated with the induced energy E and the specific heat C as

$$\triangle T = \frac{E}{C} \tag{3}$$

Then the temperature increase $\triangle T(z)$ yields

$$\Delta T(z) = \frac{(1-R)Q}{A_s \zeta C} \mathrm{e}^{-\frac{z}{\zeta}} \tag{4}$$

The temperature is assumed to be homogeneously distributed in the plane and exponentially decaying in the thickness direction z with $\mathrm{e}^{-\frac{z}{\zeta}}$ as seen in Eq. (4). One example of the temperature rise in aluminum is represented in Fig. 2, where a laser pulse with 100fs duration (full width at half maximum), an intensity of 2.45 J/m^2 and an irradiated spot size of 50 μm in diameter is used. At a distance z equal to the absorption length ζ the induced temperature drops to 40% of the temperature increase at the surface. The temperature increases at a distance of three times the absorption length 3ζ amounts to only 5%. In other words, the temperature is affected only within a region of three times the absorption length ζ by the incident pump pulse. Fig. 2 shows that the induced temperature change in copper and aluminum is similar but

Table 1 Material property of Al and Cu

Material	Specific heat [10^6 J/mm^3] C	Reflectivity R	Thermal Expansion [10^6/K]α	Penetration depth [nm]
Aluminum	2.42	0.87	23.1	7.54
Copper	3.45	0.96	16.5	12.65

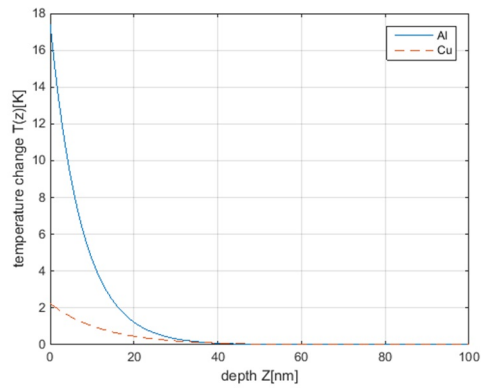

Fig. 2 Temperature distribution induced by ultra-short laser pulse in aluminum and copper

the temperature increase in copper is very small compared to the changes in aluminum. It is mainly caused by the higher optical reflectivity of copper and aluminum (Table 1). The calculations in Fig. 2 are obtained with Eq. (4) and the values in Table 1. Additional effect such as heat diffusion is not taken into account in this model.

The stress-strain-temperature relations which correspond to a generalization of the Hooke-Duhamel law is

$$\sigma_{ij} = C_{ijkl}\varepsilon_{kl} - C_{ijkl}\alpha_{kd}\triangle T \tag{5}$$

in which ε_{kl} are the components of the strain tensor, σ_{ij} the components of the stress tensor, C_{ijkl} the elastic compliance tensor, $\triangle T$ the temperature increase and α_{kl} the coefficients of linear thermal expansion, which constitute a diagonal-symmetric tensor. Assuming isotropic linear elastic material, the stiffness tensor C_{ijkl} is replaced by λ and μ as Lamé constants. Since the spot size is very large compared with

the absorption length ζ, and film thickness d, the only nonzero component of the strain tensor is $\varepsilon_z(z)$ and therefore, Eq. (5) can be reduced to

$$\sigma_z(z) = (\lambda + 2\mu)\varepsilon_z(z) - (3\lambda + 2\mu)\alpha\Delta\mathrm{T(z)} \tag{6}$$

So, the stress σ_z in the material consists of a mechanical part $\sigma_{z,Mech}$ and a thermal part $\sigma_{z,Therm}$.

$$\sigma_z = \sigma_{z,Mech} + \sigma_{z,Therm} \tag{7}$$

The thermal stress $\sigma_{z,Therm}$ is caused by the instantaneous temperature rise $\triangle T(z,t)$, which is according to Eq. (7)

$$\sigma_{z,Therm} = -(3\lambda + 2\mu)\alpha \triangle T(z) \tag{8}$$

With the equation of motion of the only component z, the kinematic relation becomes

$$\rho\frac{\partial^2 u_z}{\partial t^2} = \frac{\partial \sigma_z}{\partial z} \quad \text{and} \quad \varepsilon_z = \frac{\partial u_z}{\partial z} \tag{9}$$

From Eq. (8) and (9), the strain component caused by the propagating acoustic pulse and the time independent strain component caused by the thermal expansion can be calculated with a stress free boundary condition at the surface of the material [7,8].

$$\varepsilon_z(z,t) = \frac{\alpha(1-R)Q}{\zeta C}\frac{(3\lambda+2\mu)}{(\lambda+2\mu)}\left\{e^{\frac{z}{\zeta}}\left(1-\frac{1}{2}e^{\frac{c_l t}{\zeta}}\right)-\frac{1}{2}\mathrm{sgn}(z-c_l t)e^{-\frac{|z-c_l t|}{\zeta}}\right\} \tag{10}$$

The strain pulse propagating in thickness direction (z direction, Fig. 3) with the longitudinal wave velocity c_l, is determined by the Lamé constants and the density of the film as follows

$$c_l = \sqrt{\frac{\lambda + 2\mu}{\rho}} \tag{11}$$

In Eq. (10), it is also assumed that the temperature rise occurs instantaneously and that after this rise temperature remains constant. This assumption remains valid when the strain pulse moves much less than the spatial length of strain pulse and the penetration depth ζ during the duration of laser pulse. Usually the grains of the polycrystalline metals have arbitrary orientation. The diameter of the irradiated spot size on the surface of the material is 2 or 3 orders of magnitude larger than the grain size. So the bulk acoustic wave velocity c_l can be assumed a constant in the direction of propagation plane. The quantitative results in Fig. 3 are based on the induced temperature change presented in Fig. 2 and the corresponding laser parameters, as well as the mechanical properties of materials in Table 1. Fig. 3(a) displays the strain pulse at 5 ps after the laser

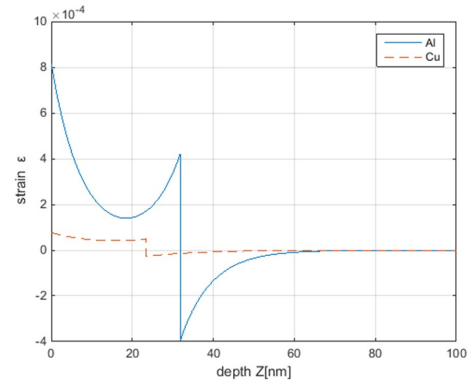

(a)

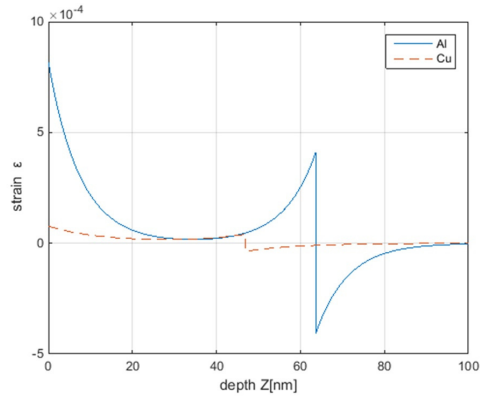

(b)

Fig. 3 Illustration of the propagation of the ultrasonic pulses in aluminum and copper after (a) 5 picoseconds, (b) 10 picoseconds

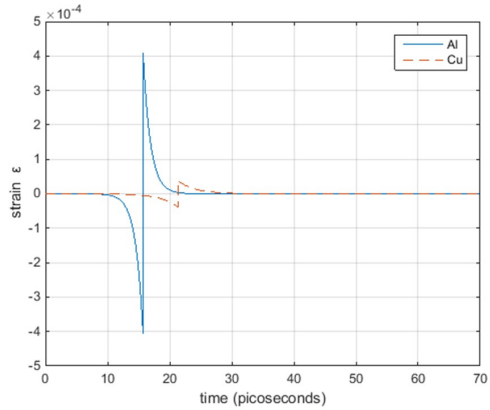

Fig. 4 Strain pulses at z=100nm from the free surface of aluminum and copper

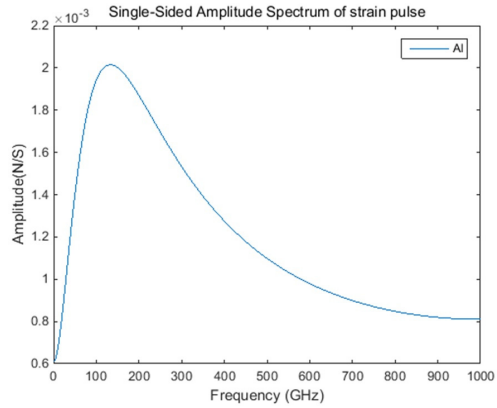

Fig. 5 Frequency spectrum of the strain pulse at 100nm from the free surface

pulse is incident on the surface, while Fig. 3(b) represents the strain pulse at 10 ps after the laser pulse is incident on the free surface. Aluminum shows the higher bulk wave speed than copper. Also the amplitude of the generated acoustic pulse of Al is larger than the pulse shape of copper due to the bigger thermal expansion coefficient.

According to Fig. 3 the strain distribution in the materials can be divided into two parts: a static part due to the thermal expansion near the free surface and a propagating part. The propagating strain pulse again consists of two equal components with opposite signs: During the absorption of the laser pulse one part is propagating directly in the positive thickness direction z (part with negative strain) during the absorption of the laser pulse and one originally propagating in the negative direction ($-z$). The second one is instantaneously reflected at the stress-free boundary, therefore its strain is positive. The acoustic wavelength of the strain pulse is an order of 10 nm as shown in Fig. 3, whereas the pulse width is about 10 picoseconds in time scale as in Fig. 4. The spectrum of this pulse travelling from the boundary into the medium is illustrated in Fig. 5 for aluminum, where it contains hundreds of GHz components spanning up to THz domain.

3. Numerical Calculation of 1-D Elastic Wave Propagation

Previous analytical model gives a fast but rough calculation of the pico-second acoustic pulse without extensive works. But it is not able to compute the excitation and propagation of ultrasound in microstructures with complex shape. Unlike analytical models, numerical models are more flexible for describing the travelling wave in specimens consisting of a stack of various layers. For the calculation of hyperbolic differential equations like the wave Eq. (9) it is well known to be not worthy to use implicit algorithms. Therefore, in this paper, an explicit staggered algorithm is implemented for computational efficiency. The staggered algorithm has the advantage of the simple implementation of the boundary condition and in addition this algorithm can also be used in 2D or 3D problems [13].

If the derivative with respect to time of the stress-strain relation and the strain-displacement relation of Eq. (9) is used, we get the following set of differential equations:

Wave equation (Newton):

$$\rho \frac{\partial^2 u_z}{\partial t^2} = \frac{\partial \sigma_z}{\partial z} \quad \text{and} \quad \varepsilon_z = \frac{\partial u_z}{\partial z} \tag{12}$$

Stress-strain relation:

$$\frac{\partial \sigma_z(z)}{\partial t} = (\lambda + 2\mu)\frac{\partial \varepsilon_z(z)}{\partial t} - (3\lambda + 2\mu)\alpha \frac{\partial}{\partial t}[\Delta T(z,t)] \quad (13)$$

Strain-displacement relation:

$$\frac{\partial \varepsilon_z}{\partial t} = \frac{\partial^2 u_z}{\partial t \partial z} \quad (14)$$

If the velocity is expressed by $\frac{\partial u_z}{\partial t} = v_z$, above equations get combined and reduced to the following set of equations.

$$\frac{\partial v_z}{\partial t} = \frac{1}{\rho}\frac{\partial \sigma_z}{\partial z} \quad (15)$$

$$\frac{\partial \sigma_z}{\partial t} = (\lambda + 2\mu)\frac{\partial v_z}{\partial z} - (3\lambda + 2\mu)\alpha \frac{\partial}{\partial t}[\Delta T(z,t)] \quad (16)$$

Or substituting Eq. (15) into Eq. (16) gives

$$\frac{\partial^2 \sigma_z}{\partial t^2} = \frac{(\lambda + 2\mu)}{\rho}\frac{\partial^2 \sigma_z}{\partial z^2} - (3\lambda + 2\mu)\alpha \frac{\partial^2}{\partial t^2}[\Delta T(z,t)] \quad (17)$$

It is clearly seen from Eq. (17) that the strain pulse propagates with longitudinal wave velocity $c_l = \sqrt{\frac{(\lambda + 2\mu)}{\rho}}$ after the thermal disturbance $\triangle T(z,t)$ is applied. For numerical solution of the simultaneous Eqs. (15) and (16), both equations are discretized in the time and space domain. In the space domain the 1-D grid is used for the z-direction of the thickness in the material. The superscripts c, r and l denote the center, right and left of the corresponding grid-node as shown in Fig. 6. The spatial discretization of Eq. (15) and (16) can be written as follows

$$\frac{\partial v_z^c}{\partial t} \approx \frac{1}{\rho}\frac{\sigma_z^r - \sigma_z^l}{\Delta z} \quad (18)$$

$$\frac{\partial \sigma_z^c}{\partial t} \approx (\lambda + 2\mu)\frac{v_z^r - v_z^l}{\Delta z} - (3\lambda + 2\mu)\alpha \frac{\partial}{\partial t}[\Delta T(z,t)] \quad (19)$$

The temporal discretization is made by Taylor's central approximation.

$$\frac{\partial f}{\partial t} \approx \frac{f(t+\Delta t) - f(t-\Delta t)}{2\Delta t}, \quad (20)$$

or $f(t+\Delta t) \approx f(t-\Delta t) + \dot{f} \cdot 2\Delta t$

$$v_z(t) \approx v_z(t-\Delta t) + \dot{v}_z(t - \frac{\Delta t}{2})\Delta t \quad (21)$$

$$\sigma_z(t + \frac{\Delta t}{2}) \approx \sigma_z(t - \frac{\Delta t}{2}) + \dot{\sigma}_z(t)\Delta t \quad (22)$$

The finite difference Eqs. (20)-(22) approximated by truncated Taylor series needs to choose the right step size in time and space domain for reducing numerical dispersion and errors. To avoid the exponential growth of the amplitude during calculation, a critical time step $\triangle t$ governed by the Neumann stability analysis was adopted to this one dimensional analysis such that [14],

$$\Delta t \le \frac{\Delta z}{c_l} \quad (23)$$

On a stress free boundary shown in Fig. 6, the stress in normal direction vanishes at the surface where the laser pulse is incident. In order for this boundary condition to be satisfied, an additional imaginary grid point just out of the medium surface is set to negative value of the first stress node $\sigma_z(1,t)$ inside the material. The approximation of the velocity is determined by the interpolation of the neighboring stress grid points in Eq. (18).

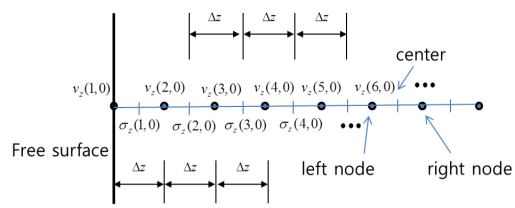

Fig. 6 One dimensional discretization of spatial domain at t=0

4. Simulation Results and Discussion

The numerical scheme presented in this work was applied to two cases for the simulation of excitation and propagation of picosecond ultrasound, one of which is a 1-D homogeneous isotropic unbounded medium and the other is a 1-D half-space $z \geq 0$ with free boundary surface as shown in Fig. 7.

Laser pulse used in Fig. 7 (a) and (b) has the same characteristic of the laser given by Fig. 2 in the analytical analysis. In the unbounded medium (Al) of Fig. 7(a), a heat source of laser pulse is located inside the material and applied for a very short time to excite acoustic wave. Temperature distribution by the ultrafast laser source is assumed to have an inversed Garbor function as shown in Fig. 8, where a stress (negative) distribution is represented with the distance from the center of heat source.

Starting the numerical calculation presented in the previous section with initial condition of stress given by Fig. 8, particle velocities of all nodes after a time interval $\triangle t$ are determined first from the dynamic relation between stress and velocity given in Eq. (15). Then velocity values are substituted into discretized equation (16) for calculation of stress at next time step. This sequence of calculation is performed by Matlab until a certain amount of time (30 ps). One example is displayed in Fig. 9 to show the propagation of an acoustic pulse generated by initial thermal stress of Fig. 8 in 1-D unbounded medium. In Fig. 9, initial stress distribution of Fig. 8 is split into two stress pulses of same shape in spatial domain and spread over the medium with longitudinal wave velocity. Fig 9(a) represents two acoustic pulses same but propagating in opposite direction at 2 ps after the laser pulse is applied. Fig. 8(b) and (c) illustrate the same acoustic pulses propagating after 6 and 8 pico-seconds (ps) respectively after

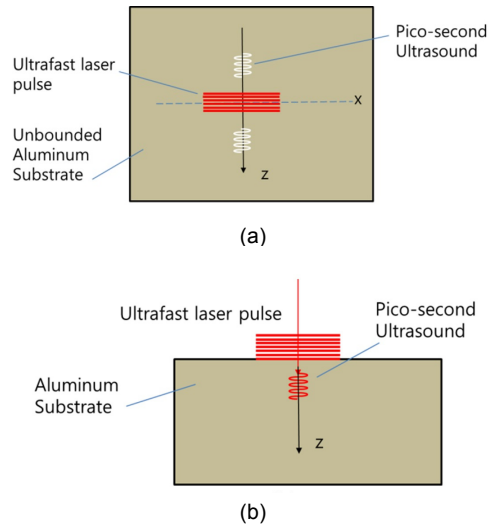

Fig. 7 Acoustic excitation in (a) an unbounded, (b) a half-bounded medium with free surface

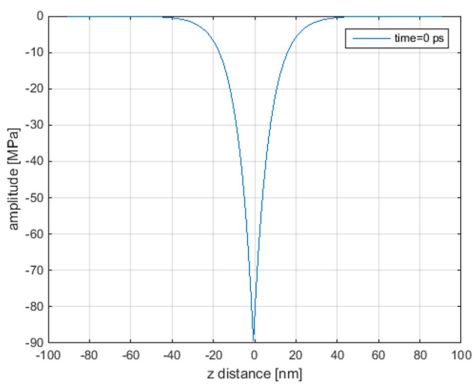

Fig. 8 Stress distribution induced by temperature rise from laser puls

the laser pulse is illuminated. Fig. 9(d) displays three dimensional representation of the propagating acoustic pulses of Fig 9(a)-(c), where stress in vertical axis is drawn versus spatial and temporal axis. It is also seen from the figures that a wiggling noisy signal is produced at the center and magnified with the increase of propagation time and distance. It is caused mainly by singular point at the peak in the center of Fig. 8 where no derivatives exist. Error in FD approximation at this singular point increases and propagates as the time step proceeds.

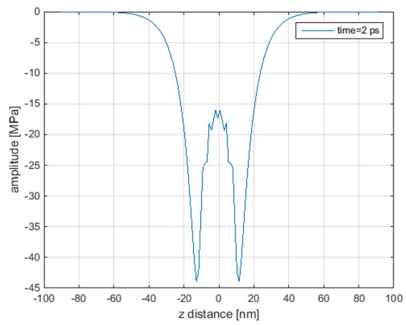

(a)

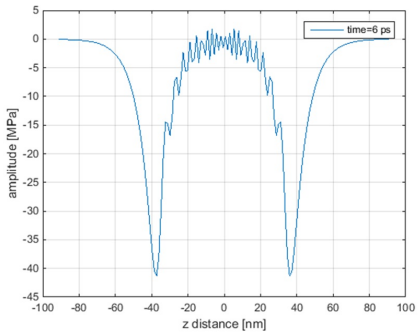

(b)

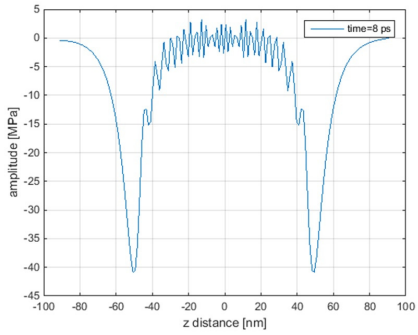

(c)

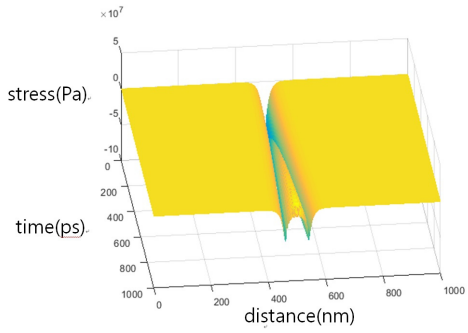

(d)

Fig. 9 Propagation of acoustic pulse in 1-D isotropic unbounded medium(Al) after laser pulse is applied, (a) 2 ps, (b) 6 ps, (c) 8 ps, (d) 3D visualization

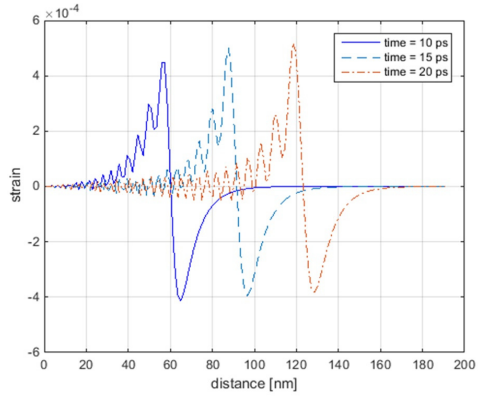

Fig. 10 Propagation of acoustic pulse in 1-D isotropic half-bounded medium(Al) after laser pulse is applied on its surface

Next Fig. 10 shows the bulk wave propagations in a half-bounded aluminum substrate in Fig. 7(b) calculated with the presented FD method. In Fig. 10, three consecutive acoustic pulses from 10ps to 20 ps after the laser pulse is hit are displayed simultaneously for comparison. In Fig. 10, x-axis represents the distance from free surface of medium and y-axis indicates strain. Each pulse has almost the same pulse shape of nano-order width and travels with the longitudinal wave velocity $c_l = 6360\ m/\mathrm{sec}$. It is also obvious that the travelling acoustic pulse has high frequency content which is caused by the abrupt sign change. For the presented numerical results a time step $\triangle t$ of 2fs was chosen. The spatial step size of the grid in the media was determined by the wave speed c_l and the time step $\triangle t$ of Equation (23). Numerical solution of Fig. 10 is little different from the analytical solution of the wave equation in Fig. 3. Unlike the analytical solution, it shows a smooth peaks and errors in magnitude and phase appearing as a smearing and wiggling of waveforms. It is because of numerical dissipation and dispersion occurring during FD discretization in space and time domain. For instance, when comparing the amplitude of the analytical solution (Fig. 3) and the numerically calculated

results (Fig. 10) far enough from the surface, the propagating strain pulses of the peak-peak amplitude of $\pm 4.3E10^{-4}$ in Fig. 10 should have an amplitude of $\pm 4E10^{-4}$ as in the analytical solution (Fig. 3). This is partly because the spatial grid is slightly too rough for sampling the sharp positive and negative peaks occurring at the sign change of the travelling acoustic pulse. Even though there are numerical algorithms to reduce or eliminate the numerical errors by means of advanced FDM methods such as Lax-Wendroff or Crank-Nicolson scheme, the results obtained in this analysis without such numerical optimization is acceptable for the purpose of understanding the generation of picosecond ultrasound. By reducing the temporal and the spatial step size as well, this inaccuracy of the sampling can nearly be eliminated and will be covered in future work.

5. Conclusions

Excitation and propagation of an ultrasound with nano-scale wavelength realized by using ultrafast laser technique is described using a mathematical model and simulated by numerical method. The laser pulse in the order of 100 femtoseconds applied to the surface of aluminum substrate excites the free electron of material leading to lattice vibration, which turns into acoustic pulse. Analytical model combines the energy transfer from optical photon to phonon with elasto-dynamic wave equation to calculate the strain pulse induced by ultrafast laser pulse in 1-D half-bounded medium of copper and aluminum. Analytical solution shows that the excited acoustic pulse is the longitudinal wave with extremely high frequencies up to THz and a very short wavelength of 10 nm order. So it can be employed for the time-of-flight measurement to characterize thin films and microstructures. Apart from the analytical thermo-mechanical model, numerical models using finite differences (FD) for describing the transient heating after absorption of the laser pulse are implemented to investigate the generation and propagation of bulk acoustic waves in two cases of boundary conditions such as 1-D unbounded and half-bounded medium. The proposed FD techniques are successfully applied and found effective to calculate the bulk waves and characterize acoustic pulses. It can be concluded from the simulation results that the velocity of the acoustic pulse is measured easily from TOF of pico-second bulk wave to calculate the thickness or material properties such as Young's modulus of thin films in microstructures.

Acknowledgments

Authors gratefully acknowledge the support to this work partly by Korea University of Technology and Education and Radiation Technology R&D program through the National Research Foundation of Korea funded by the Ministry of Science, ICT & Future Planning NRF-2013M2A2A9043274

References

[1] C. S. Kim and I. Park, "Review of Micro/Nano nondestructive evaluation technique(I): surface and subsurface investigation," *Journal of the Korean Society for Nondestructive Testing*, Vol. 32, No. 2, pp. 198-209 (2012)

[2] C. S. Kim and I. Park, "Review of Micro/Nano nondestructive evaluation technique(II): measurement of acoustic properties," *Journal of the Korean Society for Nondestructive Testing*, Vol. 32, No. 4, pp. 418-430 (2012)

[3] S. Anisimov, B. L. Kapeliovich and T. L. Perel'man, "Electron emission from metal surfaces exposed to ultrashort laser pulses," *Soviet Phys. JETP*, Vol. 39, No. 2, pp. 375-377 (1974)

[4] T. Q. Qiu and C. L. Tien, "Short-pulse laser heating on metals," *International Journal of Heat and Mass Transfer*, Vol. 35, No. 3, pp. 719-726 (1992)

[5] B. Bonello, B. Perrin, E. Romatet and J. C. Jeannet, "Application of the picosecond ultrasonic technique to the study of elastic and time-resolved thermal properties of materials," *Ultrasonics*, Vol. 35, pp. 223-231 (1997)

[6] C. Thomsen, J. Strait, Z. Vardeny, H. J. Maris, J. Tauc and J. J. Hauser, "Coherent phonon generation and detection by picosecond light pulses," *Physical Review Letters*, Vol. 53, No. 10, pp. 989-992 (1984)

[7] C. Thomsen, H. T. Grahn, H. J. Maris and J. Tauc, "Surface generation and detection of phonons by picosecond light pulses," *Physical Review B*, Vol. 34, No. 6, pp. 4129-4138 (1986)

[8] J. K. Chen, W. P. Latham and J. E. Beraun, "Axisymmetric modeling of femtosecond-pulse laser heating on metal films," Numerical Heat Transfer, Part B, Vol. 42, pp. 1-17 (2002)

[9] J. K. Chen, J. E. Beraun and C. L. Tham, "Investigation of thermal response caused by pulse laser heating," Numerical Heat Transfer, Part A, Vol. 44, pp. 705-722 (2003)

[10] Y. C. Lee, K. C. Bretz, F. W. Wise and W. Sachse, "Picosecond acoustic measurements of longitudinal wave velocity of submicron polymer films," *Applied Physics Letters*, Vol. 69, No. 12, pp. 1692-1694 (1996)

[11] D. M. Profunser, J. Vollmann, J. Bryner and J. Dual, "Measurement and simulation of the laser-based thermo-elastic excitation and propagation of acoustic pulses for thin film and MEMS inspection," *Proc. SPIE* Vol. 4703, pp. 21-30 (2002)

[12] T. F. Leutenegger, "Detection of defects in cylindrical structures using a time reverse numerical simulation method," Diss. ETH No. 14833, Zürich (2002)

[13] F. Schubert, A. Peiffer, B. Kohler and T. Sanderson, "The elastodynamic finite integration technique for waves in cylindrical geometries," *Journal of the Acoustical Society of America*, Vol. 104, No. 5, pp. 2604-2614 (1998)

[14] H. Koh, "A study on the source and boundary modeling finite difference time domain method for solving acoustic problems," MS thesis, KAIST (2006)